Research Square

Preprints are preliminary reports that have not undergone peer review.
They should not be considered conclusive, used to inform clinical practice,
or referenced by the media as validated information.

Ozone-induced yield losses for winter wheat at a high-altitude site in western India

Sompriti Deb Roy

sompriti@tropmet.res.in

Indian Institute of Tropical Meteorology

Vrinda Anand

Indian Institute of Tropical Meteorology

Bandarusatya Murthy

Indian Institute of Tropical Meteorology

Article

Keywords: Ozone pollution, Regional transport, High-altitude wheat loss, Exposure metrics, Economic valuation

Posted Date: November 12th, 2026

DOI: https://doi.org/10.21203/rs.3.rs-11192843/v1

License: This work is licensed under a Creative Commons Attribution 4.0 International License.
Read Full License

Additional Declarations: No competing interests reported.

Ozone-induced yield losses for winter wheat at a high-altitude site in western India

Sompriti Deb Roy[a*], Vrinda Anand[a] and Bandarusatya Murthy[a]

[a]Indian Institute of Tropical Meteorology (IITM), Pune-411008, Maharashtra, India

Email addresses: sompriti@tropmet.res.in (Sompriti Deb Roy), vrinda.anand@tropmet.res.in (Vrinda Anand), murthy@tropmet.res.in (Bandarusatya Murthy)

[*]Corresponding author: Sompriti Deb Roy (sompriti@tropmet.res.in)

Indian Institute of Tropical Meteorology, Pune-411008, Maharashtra, India

PHONE: +91-20-2590-4200, FAX : +91-20-2586-5142

Abstract

This study presents the first observational assessment of ozone-induced yield and economic losses for winter wheat at the high-altitude site of Mahabaleshwar (1353 m asl) in the Western Ghats of India. Using continuous surface ozone observations (2018–2019) from the MAPAN network, we evaluate linear metric (M7) and cumulative exposure indices (AOT40, W126). Unlike emission-driven lowland plains, this transport-dominated mountain plateau lacks nocturnal nitric oxide titration, sustaining a high ozone baseline that subjects crops to continuous, day-and-night oxidative stress. Applying established exposure-response functions, standard cumulative indices mathematically over-accumulate exposure on flat diurnal curves, projecting unrealistic theoretical relative yield losses (RYL) up to 79%. By establishing a biologically and agronomically realistic upper boundary of %RYL at 45–46% to account for active stomatal defense and harvesting failure thresholds, the %RYL is constrained to 22–46%. Under this capped framework, the annual wheat production deficit ranges from 169 to 634 tonnes (t) (21.5–46%), corresponding to a regional economic deficit of USD 0.03–0.15 million. These findings demonstrate that remote high-altitude agricultural vulnerability is decoupled from local emissions, highlighting the urgent need for transboundary air quality management, region-specific exposure-response functions, and cultivar-specific flux-response relationships.

Keywords *Ozone pollution, Regional transport, High-altitude wheat loss, Exposure metrics, Economic valuation*

Introduction

Tropospheric ozone (O3) is a secondary phytotoxic pollutant that adversely affects plant physiology by inducing oxidative stress following stomatal uptake. This exposure generates Reactive Oxygen Species (ROS) and impairs enzymes such as Rubisco, leading to reduced carbon assimilation, photosynthetic efficiency, accelerated leaf senescence, and ultimately, measurable crop yield losses [1–8]. To quantify these impacts, exposure-based metrics such as AOT40 and W126, along with concentration-based indices like M7, are widely used to assess the ozone exposure effects influencing crop response [9–12].

Surface ozone levels that dictate these metrics are governed by the interplay of precursor emissions, meteorological conditions, atmospheric chemistry, and transport processes. Sharp regional contrasts exist between emission-driven urban regions and transport-dominated remote environments. In South Asia, rapid urbanization and industrial expansion have increased emissions of ozone precursors, resulting in elevated and spatially heterogeneous ozone levels [13–15]. Consequently, several studies have quantified ozone-induced crop losses using both modeled and observational approaches [16–20].

However, these assessments predominantly focus on lowland agricultural regions such as the Indo-Gangetic Plains, where local photochemical production and NOx/VOC limitations govern ozone variability [21–23]. These lowland studies fundamentally assume an emission-driven atmospheric regime characterized by strong daytime photochemical build-up and nocturnal depletion. In contrast, high-altitude regions represent a distinct atmospheric regime where surface ozone is primarily controlled by regional and long-range transport, along with stratosphere–troposphere exchange, rather than local photochemical production [24–26].

Without the nocturnal NOx titration typical of urban plains, these transport-dominated mechanisms sustain elevated baseline ozone concentrations throughout the diurnal cycle, particularly during the dry winter cropping seasons. Consequently, high-altitude crops face persistent, chronic oxidative stress that differs fundamentally from the acute, daytime-only exposure events characterizing lowland agriculture [27, 28].

Despite this unique physical mechanism, high-altitude agricultural environments where ozone is governed primarily by transport processes remain largely uncharacterized in terms of crop impacts using observational data. Addressing this gap is necessary because elevated background ozone in these regions is decoupled from local emission controls. This implies that high-elevation crops may suffer persistent yield degradation even in the absence of proximate industrial or vehicular pollution. Furthermore, applying standard non-linear cumulative metrics (such as AOT40 and W126) to these flat, non-titrating diurnal curves leads to extreme, unrealistic theoretical yield loss projections (as high as 79%), creating a critical need for a realistic, physiologically and agronomically bounded framework to resolve this metric non-uniqueness. Since ozone concentrations persistently hover above standard thresholds (e.g., 40 ppb), the cumulative metrics over-accumulate exposure non-linearly. The lack of site-specific observational assessments in these transport-dominated, high-elevation zones leaves a critical gap in regional food security assessment.

To address these gaps, the present study provides the first continuous, observation-based assessment of ozone-induced crop yield and economic losses for winter wheat at the high-elevation site of Mahabaleshwar (1353 m above sea level) in the Western Ghats of India, using ground-based monitoring data from the MAPAN network for the period 2018–2019.

This work makes three key scientific contributions:

- First, High-Altitude Observational Assessment: We quantify the in-situ ozone-induced agricultural risks in a unique high-altitude transport-dominated regime, showing that crop vulnerability persists even in a remote environment decoupled from local anthropogenic emission sources.

- Quantification of Metric Divergence and Non-Uniqueness: We systematically evaluate how linear concentration-based (M7) and non-linear cumulative exposure-based (AOT40 and W126) metric formulations behave when applied to flat diurnal curves, demonstrating that standard cumulative non-linear metrics mathematically amplify exposure values and yield loss estimates.

- Formulation of a Physiologically and Agronomically Bounded Capped framework: We establish a biologically and economically realistic capped framework (setting a %RYL cap of 45–46% to account for plant stomatal closure and harvesting failure thresholds), resolving the mathematical overestimation of

standard cumulative metrics and providing a robust, realistic range of regional production and economic deficits.

Materials and methods

Site description

The monitoring site is located at the high-altitude station of the Indian Institute of Tropical Meteorology (IITM) in Mahabaleshwar (17º55'30", 73º39'36"E), situated within the Western Ghats Mountain range in the Satara district of Maharashtra, India, at an elevation of 1353m above sea level (asl). The topography of Mahabaleshwar is characterized by an extensive plateau surrounded by deep valleys on all sides, exposing the site to free-tropospheric air masses and regional transport plumes [29].

The local climatology is classified as humid subtropical/tropical monsoon subtropical with very heavy rainfall in the monsoon period (June–September) and relatively dry conditions during winter (December–February), coinciding with the wheat-growing season. The coldest month is January with an average temperature of 19.8°C, and the warmest month is April with an average temperature of 25.3°C. The average annual rainfall is 2212 mm, and the average annual temperature is 21.9°C. The wettest month is July with an average of 714 mm of rainfall, and the driest month is January with around 1mm of rainfall. The four major seasons are summer (March to May), Monsoon (June to September), post-monsoon (October to November), and winter (December to February).

The wind climatology at this high-altitude station exhibits distinct deviations from the regional lowland patterns. During winter, southeasterly winds predominate, supplemented by occasional northwesterly and southwesterly flows. In the pre-monsoon season, westerly and northwesterly winds dominate, which, combined with convective boundary layer growth, facilitate the regional and long-range transport of continental air masses to the plateau [29, 30]. In the monsoon months, prevailing winds are mostly westerly and northwesterly, and during the post-monsoon period, the winds are mainly southeasterly.

The monitoring location is a well-known tourist spot with not many industries nearby and is around 260 km from the densely populated and industrialized area of Mumbai, situated towards the northwestern side of Mahabaleshwar. Located in a remote hilly forest reserve, the site has pleasantly cool weather throughout the year and minimal local

industrial or vehicular emission sources, making its atmospheric chemistry highly representative of rural background and transported pollution regimes in western India [31].

Analytical details

Surface ozone (O_3) mixing ratios were measured continuously at an hourly frequency using a commercial photometric ozone analyzer [32]. The analyzer operates on the physical principle of ultraviolet (UV) absorption at 253.7nm, where the attenuation of light through a sample cell is compared to a reference ozone-free air sample to calculate the mixing ratio via the Beer-Lambert law [32]. The instrument has a measurement range of 0.001-10ppm, a lower detection limit of 1ppb (0.001ppm), and an accuracy of ±2%. Regular calibration and span checks were performed periodically following the standardized protocols outlined by Mallik et al. [33].

To ensure high-quality data, raw observations collected at 15-minute intervals were aggregated into hourly averages and subjected to a strict quality assurance and quality control (QA/QC) protocol. Hourly values of O3 were subjected to pre-processing to filter out spikes, unrealistic values, and gaps by excluding those values that are above or below (±2σ), where σ is the standard deviation (based on the daily mean). Data filtering includes removal of outliers beyond ±2σ and exclusion of invalid or missing values. The data are further averaged for the daily mean or the 8-hourly mean. Further details on instrumentation, calibration, and data processing at the MAPAN network stations are available in Rana et al. [34], Rahman et al. [35], Latha et al. [36], and in the instrument manual [32].

Ozone exposure metrics

To evaluate the potential impact of surface ozone on winter wheat during its cropping season (January to March), three standard exposure and concentration-based metrics (AOT40, W126, and M7) were computed using the hourly observation database.

- Accumulated Ozone Exposure over a Threshold of 40 ppb (AOT40): The AOT40 metric represents the cumulative sum of hourly daytime ozone concentrations exceeding a baseline threshold of 40 ppb, for the daylight hours with global radiation greater than or equal to 50 Wm^{-2} during the crop-growing season. In the absence of site-specific radiation measurements, daylight hours (07:00–19:00 IST with global radiation ≥ 50

Wm^{-2}) were used for the calculation of AOT40 during the cropping season in this study, following previous studies in the Indian region [37, 38].

$$AOT40 \text{ (ppb h)} = \sum_{i=1}^{n}(Ci - 40), \text{for } Ci \geq 40\ ppb \quad (1)$$

Here, 'C_i' is the hourly surface ozone mixing ratio (in ppb) during daylight hours, *'i'* corresponds to the hour index, and 'n' is the total number of daylight hours over the 3-month cropping period.

- Concentration-Based 7-Hour Mean (M7): The M7 metric is the 7-hour mean of the ozone concentrations during daytime from 9–16 hours for the full duration of the crop, considering the 3- monthly growing season. The formula for the M7 exposure index of ozone is as follows:

$$M7 \text{ (ppb)} = 1/\text{n}\sum [Ci] \text{ for } i = 1 \text{ to n; for } 09{:}00 - 15{:}59 \text{ hrs.} \quad (2)$$

Here, 'C_i' is the hourly surface ozone mixing ratio (in ppb), and 'n' is the total number of hours within the 7-hour daytime window across the 3-month growing season.

- Sigmoidally Weighted Cumulative Index (W126): The cumulative index 'W126' is defined as the sum of the hourly ozone mixing ratios (weighted by a sigmoidal weighting function) accumulated over a daylight period of 12 hours from 8:00 a.m. to 7:00 p.m. (local standard time) for the 3-month crop growing period. The metric W126 does not have a threshold value like AOT40 but gives lower weight to lower concentrations and higher weight to higher concentrations based on a weighting function [12]. The daily index value (D.I.) is expressed as the daily sum of the sigmoidally weighted daylight hourly concentrations for the 12 hours (08:00–19:59 hrs.). The monthly index value (M.I.) is the sum of the daily index values for a particular month. The 3-month sum is calculated as the sum of the 3 monthly index values for the consecutive 3-month crop growing period. The formula for W126 is given below.

$$W126\ (ppm\ h) = \sum_{i=1}^{n}\left[\frac{Ci}{1+4403\exp(-126.Ci)}\right] \text{ for } Ci \geq 0 \text{ ppmv} \quad (3)$$

Here, 'Ci' is the hourly surface ozone concentration in ppm, 'i' is the hour index, and 'n' is the number of hours in the crop growing season.

Crop yield, crop loss, and economic loss calculations

To translate these exposure metrics into crop losses and economic impacts, established exposure-response (E-R) functions developed for wheat cultivars were applied. The Relative Yield (RY) represents the ratio of the actual yield to the theoretical yield in the absence of ozone damage, calculated using the following equations (4) to (6).

For Wheat:

$$RY = \exp\{-(M7/137)^{2.34}\} / \exp\{-(25/137)^{2.34}\} \quad [9] \quad (4)$$

$$RY = -0.0000161 \times AOT40 + 0.99 \quad [11] \quad (5)$$

$$RY = \exp[-(W126/51.2)^{1.747}] \quad [10] \quad (6)$$

The Relative Yield Loss (RYL) is defined as the reduction in crop yield from the theoretical yield, which would have occurred in the absence of ozone-induced damage. Its formula is given below.

$$RYL = 1.0 - RY \quad (7)$$

The Crop Production Loss (CPL_i) is calculated from the RYL and the Crop Production Yield (CP_i) using the following equation, where 'i' indicates the year of calculation.

$$CPL_i = \{RYL_i / (1 - RYL_i) \times CP_i \quad (8)$$

The economic loss due to ozone-incurred damages in a financial year for any crop is expressed as the economic cost loss or economic loss (EL). The minimum EL is calculated from the minimum support prices (MSP) and the CPL for the corresponding fiscal year through the equation given below. The MSPs are the producer prices for that particular year and for that particular crop. Here, 'i' denotes the year of calculation.

$$EL_i = CPL_i \times MSP_i \quad (9)$$

Theory/calculation

A major challenge in high-altitude agricultural risk assessment is the vertical and horizontal transport and boundary layer coupling that dictate surface ozone concentrations. Unlike lowland urban plains where local photochemistry ($[O_3] \propto NO_X + VOC + h\nu$) dictates diurnal patterns, the high-altitude regime at Mahabaleshwar (1353 m asl) is decoupled from immediate surface emissions. The absence of local anthropogenic nitric oxide (NO) emissions on this forested plateau prevents nocturnal titration ($O3 + NO \rightarrow NO_2 + O_2$), resulting in a flat, persistently elevated diurnal ozone profile where concentration levels hover constantly above 40ppb [39].

In this transport-dominated regime, since the baseline ozone never drops significantly at night, cumulative formulations AOT40 and W126 continue to accumulate exposure non-linearly across the entire daylight window, regardless of whether extreme daytime peaks occur. When these indices are applied to the linear E-R functions, they project an extreme, unrealistic theoretical RYL of up to 79%.

To resolve this metric non-uniqueness and establish a realistic impact range, we formulate a physiologically and agronomically bounded framework based on two critical constraints:

- Agronomic and Harvesting Failure Thresholds: Under the crop loss equation (8), an RYL of 50% represents a critical threshold where crop production loss equals the actual harvested yield (CPL = CP). In real-world agricultural systems, crop damage nearing this 50% threshold triggers total harvesting failure (abandonment of the crop) rather than a continuously declining harvest, as the labor and operational costs of harvesting exceed the market value of the degraded crop [4].
- Biological Plant Defenses: Under chronic exposure to elevated baseline ozone, plants activate active defense mechanisms—predominantly stomatal closure—which reduces stomatal conductance and limits further internal ozone flux regardless of high ambient exposure concentrations [40, 41].

Therefore, while the linear M7 metric provides a realistic baseline yield loss of 22%, the biologically and economically feasible upper bound of RYL for the non-linear cumulative metrics must be capped between 40% and 50% (around 45–46%). This capped upper bound aligns with field-validated extreme exposure studies in India [18] (%RYL between 11–41% in Punjab and Haryana) and regional WRF-Chem modeling studies over the Indian region, which estimated the wheat %RYL of 40–50% at Mahabaleshwar [19]. The source influences are inferred based on regional climatology and prior studies [29, 30] where HYPSPLIT trajectory analysis was performed at this

location, and we avoid direct attribution in the absence of trajectory-based analysis in this study (since it is out of scope for this study based on ozone-induced crop losses). The cropping period considered for the Rabi crop (wheat) is January to March. The production per annum for the wheat crop at Mahabaleshwar has been obtained in kilogram/Hectare (Kg/H) from the district-wise crop production report.

Results

This section presents the observational findings of surface ozone (O_3) exposure indices and quantifies the winter wheat yield and economic losses at Mahabaleshwar during 2018–2019. By applying a physiologically and agronomically capped framework, we resolve the metric non-uniqueness arising from the distinct atmospheric transport regime of this high-altitude station.

Monthly ozone exposure indices

The monthly variation of the daytime concentration-based metric (M7) and cumulative exposure-based indices (AOT40, W126) for 2018–2019 is shown in Fig. 1. All three metrics (M7, AOT40, W126) exhibit consistent seasonal behavior, with maxima during winter–pre-monsoon and minima during monsoon, reflecting the dominant influence of transport and washout processes.

In Fig. 1a, we find that the monthly mean M7 values reach the primary peak in the spring month of March (77.84 ppb in 2018; 81.1 ppb in 2019), followed by a secondary maximum in the winter month of January (77.37 ppb in 2018; 75.0 ppb in 2019). The lowest values consistently occur in the monsoon month of August (18.76 ppb in 2018; 16.9 ppb in 2019). A subsidiary peak is observed during the post-monsoon month of November, which was more pronounced in 2018 (69 ppb) than in 2019 (42.3 ppb).

Fig. 1b shows that the monthly AOT40 indices attain the maximum levels of 16443 ppb h (2018) and 17737 ppb h (2019) in the pre-monsoon month of March, with secondary peaks in January of 16330 ppb h (2018) and 15633 ppb h (2019). The AOT40 values dropped to zero in the monsoon months of August 2018, July 2019, and September 2019.

In Fig. 1c, we find that the variation of the W126 monthly index (MI) shows a similar pattern as seen in the seasonal variation of the AOT40 values, as both are cumulative ozone exposure indices. The W126 monthly index (MI)

recorded close primary and secondary peaks in January and March (24.5 ppm h and 23.62 ppm h in 2018; 22.5 ppm h and 26.4 ppm h in 2019). The W126 monthly indices reached the minimum level of 0.02 ppm h in August for both years. Both cumulative indices (AOT40 and W126) displayed a post-monsoon subsidiary peak in November 2018 (AOT40: 11,877 ppb h; W126: 16.9 ppm h), which became mild subsidiary peaks in 2019, likely due to intense rainfall and associated heavy monsoon washout effects in 2019.

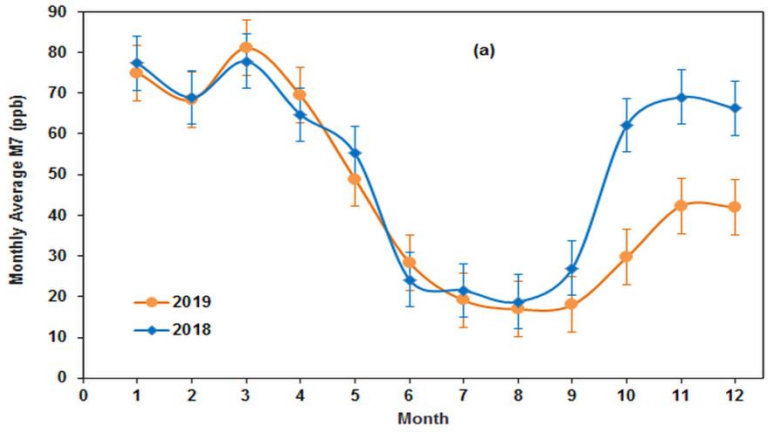


Fig. 1a Seasonal variation of the monthly mean M7 values at Mahabaleshwar for the years 2018 and 2019 with vertical error bars showing standard errors (Color on the web only)

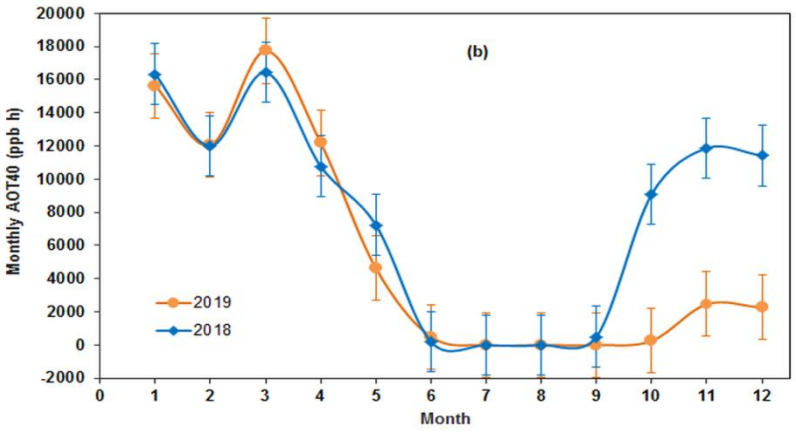
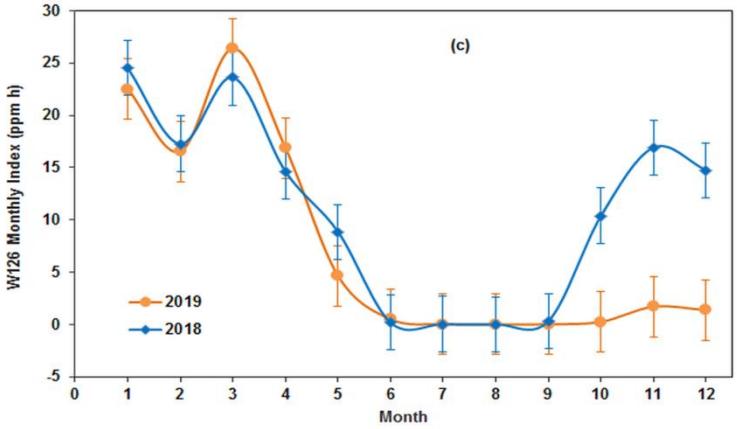


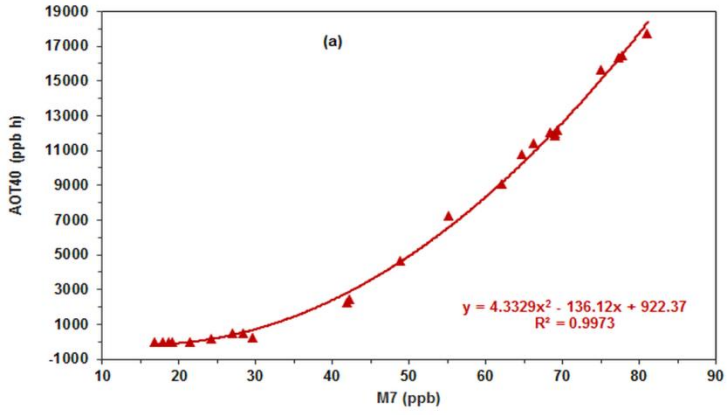
Fig. 1b Variation of monthly AOT40 values at Mahabaleshwar for the period from 2018 to 2019 with vertical standard error bars (Color on the web only)



234

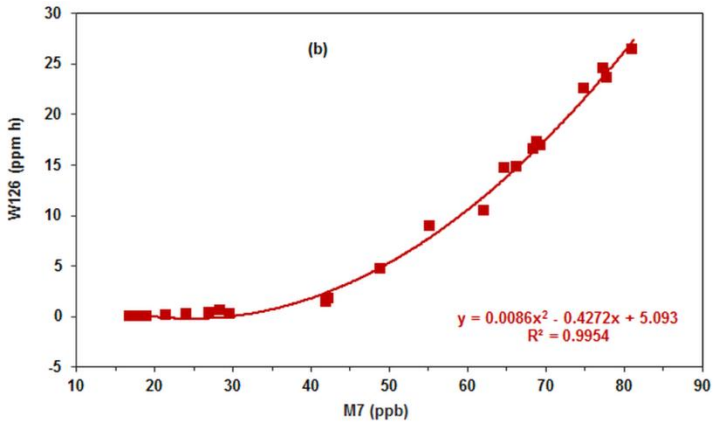
235 **Fig. 1c** Variation of monthly W126 index values at Mahabaleshwar for the period from 2018 to 2019 with vertical
236 standard error bars (Color on the web only)

237 Fig. 2a and Fig. 2b provide the relationship between the monthly average M7 values and the cumulative ozone
238 exposure indices AOT40 and W126 respectively, calculated from the observed data at Mahabaleshwar for the period
239 2018-19. In these figures, we find that a polynomial fits well between the AOT40 and M7 values ($R^2 = 0.997$) and
240 between the M7 and W126 indices ($R^2 = 0.995$). This indicates that the cumulative ozone indices are non-linear
241 transformations of ambient ozone concentrations rather than independent indicators. The non-linear amplification
242 arises from the threshold exceedances in AOT40 and weighted contributions of high-concentration episodes in
243 W126. The nonlinear transformation amplifies the variability associated with high-concentration events, resulting in
244 greater divergence in yield loss estimates.



245

246 **Fig. 2a** Relationship between the concentration-based ozone metric (M7) and cumulative exposure index (AOT40)
247 at Mahabaleshwar for 2018–2019



248

249 **Fig. 2b** Relationship between the concentration-based ozone metric (M7) and cumulative exposure index (W126) at
250 Mahabaleshwar for 2018–2019 (Color on the web only)

251 In Fig. 3a, we find that the monthly standard deviation of hourly ozone concentrations reveals pronounced seasonal
252 variability, with higher fluctuations observed during the pre-monsoon period and reduced variability during the
253 monsoon months. Interannual comparison indicates slightly higher variability in 2018 relative to 2019. This
254 temporal variability plays a critical role in cumulative exposure metrics, which are sensitive to episodic high-
255 concentration events rather than mean ozone levels. The relatively small error bars, particularly in 2019, indicate
256 that the variability observed in the ozone data is statistically robust and reflects real atmospheric processes rather
257 than sampling noise.

258 In Fig. 3b, we see that the narrow confidence intervals in the ozone data indicate high precision in the estimated
259 mean values. The absence of overlap between years 2018 and 2019 confirms a statistically significant interannual
260 difference in ozone concentration. However, the effect of these differences is relatively small compared to the
261 variation in estimated yield loss across exposure metrics, indicating that metric formulation exerts much more
262 influence on impact estimates as compared to uncertainty in ozone measurements.

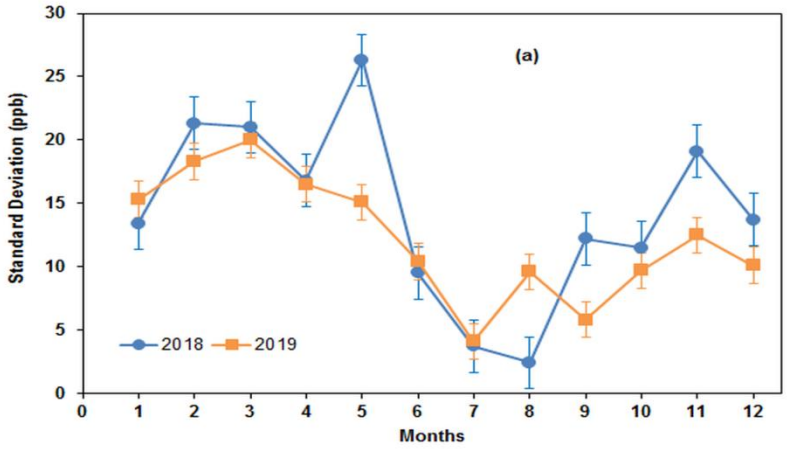


Fig. 3a Monthly standard deviation of hourly ozone concentrations with associated uncertainty at Mahabaleshwar for the years 2018–19

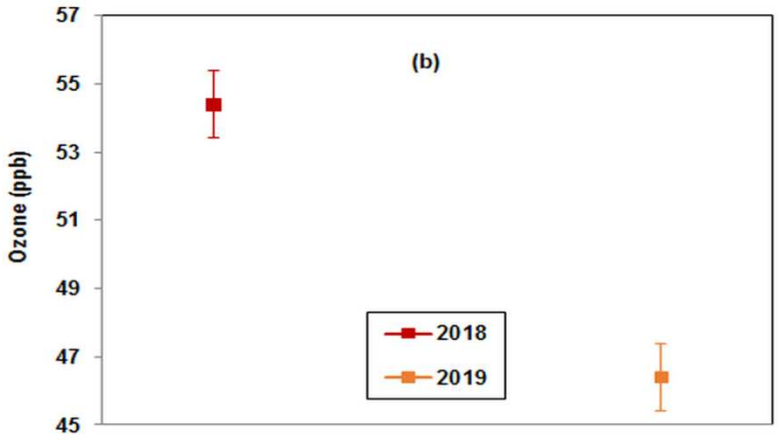


Fig. 3b Mean ozone concentrations with 95% confidence intervals for the period 2018–19 at Mahabaleshwar

Crop production loss and economic cost loss

The average M7 values have been extracted along with the integrated AOT40 and W126 values for the wheat crop, considering its cropping season (January to March), using the MAPAN data. We have applied the E-R functions to estimate the RY using equations (4) to (6), with the values obtained for M7, AOT40, and W126. The RYL has been deduced based on the estimated RY using equation (7). In the end, we have calculated the CPL and EL using the crop yield, RYL, and MSP for the wheat crop with the help of equations (8) and (9). Table 1 depicts the estimated RYL for the wheat crop at Mahabaleshwar from 2018 to 2019. The theoretical estimation of %RYL for the wheat

crop lies in the range of 22–78% and 22–79% for the years 2018 and 2019, respectively. Although the linear M7 metric provides a reasonable %RYL of 22%, the realistic agronomic upper limits of the %RYL from the non-linear metrics (AOT40 and W126) have been capped at 45% and 46%, respectively. For the wheat crop, the RYL values estimated from the concentration-based metrics (M7) are less than those calculated from the exposure indices of ozone (AOT40, W126) [17, 42, 43]. The substantially higher yield loss estimates derived from cumulative metrics (AOT40 and W126) compared to M7 indicate that threshold exceedance and sigmoidal weighting amplify the influence of high-ozone events in a non-linear manner. The annual wheat crop yields considered for the years 2018 and 2019 are 1641 Kg/H and 1973 Kg/H respectively, and the cropping period considered here is from January to March.

Year	Average M7 (ppb)	AOT40 (ppb h)	W126 (ppm h)	RYL M7	RYL AOT40 (Theoretical)	RYL W126 (Theoretical)	RYL AOT40 (Capped)	RYL W126 (Capped)
2018	74.72	44782.5	65.4	0.22	0.73	0.78	0.45	0.46
2019	74.83	45431.4	65.45	0.22	0.74	0.79	0.45	0.46

Table 1 Relative yield loss and crop yield for the wheat crop at Mahabaleshwar for the years 2018 and 2019 (Capped values represent the realistically high agronomic upper bound of %RYL (45–46%), accounting for biological limits and harvesting failure thresholds as discussed in 'Theory/ Calculation')

Table 2 gives a tabular picture of the yearly crop loss in metric tons or tonnes (t) and economic loss corresponding to the metrics applied for the wheat crop at Mahabaleshwar. Considering a realistically high agronomic upper bound of %RYL for the non-linear metrics, the annual crop loss for the wheat crop falls in the range of 169.4–527.0 t (21.5–46%) and 209.8–633.6 t (22–46.0%) for the years 2018 and 2019, respectively. The annual economic cost loss lies in the range of USD 0.03–0.12 million and USD 0.04–0.15 million for the wheat crop during the years 2018 and 2019, respectively. It is implied that the wheat crop losses at Mahabaleshwar for both the years 2018 and 2019 represent a

reasonable regional deficit. The MSPs considered for the period 2018-19 and 2019-20 are Rs.1840/ per quintal and Rs.1925/ per quintal, respectively.

Year	Crop loss M7 (t)	Crop loss AOT40 (t)	Crop loss W126 (t)	Economic loss M7 (USD)	Economic loss AOT40 (USD)	Economic loss W126 (USD)	Total Economic loss (USD)
2018	169.44	506.18	527	33648.21	111763.44	116362.48	0.03–0.12 million
2019	209.8	608.58	633.63	43586.35	140582.21	146367.38	0.04–0.15 million

Table 2 Economic cost loss for the wheat crop at Mahabaleshwar from 2018 to 2019

Table 3 shows a comparison of the crop losses estimated in this work with other relevant studies over the Indian region. Earlier, Sinha et al. [18] have calculated the losses for the wheat crop in the range of 11–41% only for the states of Punjab and Haryana in India, based on the observed data from the monitoring site at Mohali, which is consistent with our agronomically capped upper bound of 45–46% for %RYL. Avnery et al. [44, 45] have shown the %RYL for the wheat crop in India for the year 2000 to lie in the range of 8.0–30% using the global CTM (MOZART2). Our upper-bound estimate of 45–46% aligns closely with the 40–50% relative yield loss (with only the AOT40 metric) simulated over the Mahabaleshwar area by Sharma et al. [19] using high-resolution WRF-Chem modeling. Our estimates are slightly higher than the national lowland averages [38, 17], reflecting the unique physical vulnerability of high-altitude ecosystems where the absence of nocturnal titration subjects crops to continuous, day-and-night oxidative stress. Further details regarding this comparison, along with the theory and calculations of this study, are available in Deb Roy et al. [20].

Reference	Metrics used	Ozone Data	Loss of Wheat	Comments
This work	AOT40, M7 and W126	Observations	21.5–46% (AOT40, M7 and W126)	Observational data for ozone (MAPAN) at Mahabaleshwar with cropping season as given in Lal et al. [38] and Debaje [17]
Deb Roy et al. [20]	AOT40 and M7	Observations	12.4–40.8% 2.0% 4.3–20.2%	Observed ozone data (MAPAN) at Patiala with crop growing season as mentioned above Observed ozone data (MAPAN) at Tezpur with same crop growing season Observed ozone data (MAPAN) at Delhi with same crop growing season
Sharma et al. [19]	AOT40	WRF-Chem Model	21% (%RYL) 26% (%RYL)	Regional chemistry transport model with $0.3^0 \times 0.3^0$ horizontal resolution and cropping season as given in the seventh row. Crop growing season as given in the first row
Lal et al. [38]	AOT40 and M7	Observations	4.2–15%	Observed ozone data from 17 sites throughout India
Sinha et al. [18]	AOT40 and M7	Observations	11–41%	Only for Punjab and Haryana states of India with 4–4.5 month crop growing period
Debaje [17]	AOT40 and M7	Observations	5–30%	Limited observations for M7 and a relation are used to estimate AOT40.
Ghude et al. [16]	AOT40	WRF-Chem Model	5 ± 1.2%	Regional chemistry transport model with $0.5^0 \times 0.5^0$ horizontal resolution
Avnery et al. [44, 45]	AOT40 and M7	MOZART model	9.0–30% (%RYL)	Global chemistry transport model with $2.8^0 \times 2.8^0$ horizontal resolution
Van Dingenen et al. [43]	AOT40 and M7	TM5 model	13.2–27.6% (%RYL)	Global chemistry transport model with $1.0^0 \times 1.0^0$ horizontal resolution

Table 3 Comparison of crop losses estimated in this work with other related studies over India

Discussion

The absence of a sharp daytime photochemical peak [46, 39] and the persistent elevation of surface ozone throughout the diurnal cycle confirm that in situ photochemical production is not the primary driver of ozone variability at Mahabaleshwar. At lowland metropolitan or rural sites, surface ozone is heavily titrated at night by

local vehicular and industrial nitric oxide (NO) emissions ($O_3 + NO \rightarrow NO_2 + O_2$), leading to a near-zero nocturnal baseline. However, situated at 1353 m asl in a forested reserve, Mahabaleshwar lacks immediate precursor emissions to titrate ozone at night. The lack of nocturnal titration combined with strong vertical mixing creates a flat, elevated diurnal profile where ozone concentrations persistently hover above 40 ppb. This flat exposure profile subjects the winter wheat crop to continuous, chronic oxidative stress throughout the vegetative and grain-filling stages.

The diurnal baseline at Mahabaleshwar is primarily controlled by three major physical mechanisms:

- Vertical Advection and Entrainment**:** Strong daytime convective mixing entrains ozone-rich air masses from the free troposphere down into the boundary layer. This vertical coupling is enhanced during the winter and pre-monsoon spring seasons when the planetary boundary layer (PBL) grows rapidly during the daytime, tapping into the free-tropospheric ozone reservoir.

- Stratosphere–Troposphere Exchange (STE): Downward transport and subsidence of ozone-rich air from the upper troposphere and lower stratosphere, which peaks during the dry winter and pre-monsoon periods, raising the background ozone.
- Regional and Long-Range Transport: During the pre-monsoon months, the prevailing westerly and northwesterly winds help in the regional and long-range transport of pollutants. This, along with the subsidence of ozone-rich air from the upper troposphere and stratosphere, contributes to the springtime peaks of the monthly M7, AOT40, and the W126 MI values. In the winter period, the predominant northwesterly and southeasterly winds aid in the regional and long-range transport of pollutants. This, in addition to the stratospheric contribution of ozone, results in the wintertime peaks of the monthly M7 values, W126 indices, and the monthly AOT40 values during the coldest month of January. During the post-monsoon period, the prevailing south-easterly winds drive the regional transport of pollution from the biomass-burning activities occurring over the central Indian region, leading to the subsidiary peak of all the indices in the post-monsoon month of November.

Air mass trajectory analyses from previous studies indicate that the regional pollution at Mahabaleshwar is likely influenced by the biomass-burning activities occurring in areas surrounding central India and from the industrialized areas of western India [29, 30]. Over the Indian region, biomass-burning activities reach their maximum level during

the post-monsoon and winter months [47]. The long-range transport of pollutants at Mahabaleshwar has been associated with pollution from distant places like the Arabian countries, the African region, and the Thar Desert in northwestern India.

The estimated % RYL in this study is derived from standard exposure–response (E-R) functions developed primarily using North American and European crop cultivars under controlled or semi-controlled conditions [9–11]. As highlighted by Emberson et al. [48], applying these generalized relationships to South Asian agricultural systems introduces uncertainty, as they do not account for region-specific factors such as cultivar sensitivity, crop phenology, agronomic conditions, or management practices including irrigation and nutrient application. Asian cultivars frequently exhibit higher sensitivity to oxidative stress. Therefore, these estimates using the globally adopted set of E-R functions likely represent a conservative lower bound of actual physiological damage [49]. Although the flux-based approach is considered to be better than the exposure approach, especially in areas where the crops are influenced by water scarcity, the application of both approaches gave similar results in some studies [41, 50]. The study location is the high-elevation site of Mahabaleshwar, which has heavy monsoon and pleasant weather almost throughout the year. This substantially reduces the chances of the monitoring site being affected by water scarcity. While flux-based approaches account more rigorously for environmental factors driving stomatal conductance [40], exposure approaches remain the standard for regional agricultural risk assessments where detailed physiological data are unavailable. The relative yield loss (RYL) and associated economic impacts estimated in this study represent estimated ozone-induced effects rather than field-validated agricultural outcomes. A key limitation is the absence of in situ agronomic observations.

Conclusions

High-altitude agricultural zones represent unique, transport-dominated atmospheric environments where the absence of nocturnal titration sustains elevated surface ozone baseline levels year-round. Using ground-based observations from the MAPAN network at Mahabaleshwar (1353m asl), this study conducted the first systematic evaluation of ozone-induced winter wheat yield losses and economic losses in this remote, high-elevation tropical plateau.

The key scientific findings of this study are:

- Deterministic Metric Divergence: A strong nonlinear relationship is observed between the concentration-based metric M7 and the cumulative exposure metrics (AOT40 and W126), with second-order polynomial fits yielding $R^2 = 0.997$ for AOT40 and $R^2 = 0.995$ for W126. This confirms that the cumulative metrics are deterministic transformations of concentration-based ozone levels, with nonlinear amplification arising from thresholding and weighting effects. Since high-altitude locations lack nocturnal titration, baseline ozone remains persistently elevated. At these sites, the non-linear transformations of ozone concentrations play an important role in the divergence of the estimated crop impacts, highlighting the sensitivity of ozone impact assessment to non-linear metric formulation rather than uncertainty in ozone measurements.
- Resolution of Metric Non-Uniqueness: Our theoretical %RYL estimate for the wheat crop during the period (2018 to 2019) lies in the range of 22–79%. While cumulative exposure metrics project theoretical yield losses up to 79%, this extreme upper limit reflects the mathematical non-linear amplification of applying non-linear indices to flat diurnal curves in a high-altitude regime. By establishing a realistic agronomic upper limit of %RYL (45–46%) that accounts for physiological limits, plant defense mechanisms (like stomatal closure), and harvesting failure thresholds, the estimated relative yield loss (RYL) for winter wheat comes out to a realistic range of 22–46%.
- Quantification of Agricultural Deficits: Based on this capped framework, the annual crop production deficit ranges from 21.5–46% (169–634 t), resulting in an associated economic loss lying between USD 0.03–0.15 million.
- Decoupling Vulnerability and Policy Shift: Since high-altitude agricultural vulnerability is decoupled from local emissions and driven by stratosphere-troposphere exchange and regional/long-range transport, mitigating this damage for regional food security requires transboundary and inter-state air quality management rather than localized emission controls. Although this study is focused on a high-altitude site in India, other hilly sites around the world can also be influenced by such ozone-induced agricultural risk. The consistently high exposure levels and corresponding RYL estimates highlight a significant ozone-related risk to winter wheat in high-altitude environments, underscoring the need for region-specific E-R functions, field-based validation, flux-oriented assessment approaches, and the integration of vertical sounding data to fully resolve the transport of phytotoxic pollution into remote agricultural zones.

Declarations

All authors have read, understood, and have complied as applicable with the statement on "Ethical responsibilities of Authors" as found in the Instructions for Authors.

Funding

The MAPAN data which was used in this work was financially supported by the MoES (Ministry of Earth Sciences), India. No sponsors were involved as funding sources for the conduct of this research work.

Competing interests

The authors have no relevant financial or non-financial interests to disclose. The authors have no competing interests to declare that are relevant to the content of this article.

Authors' contribution

All authors contributed to the study conception, methodology, design, and visualization. Data acquisition was performed by Vrinda Anand. Data analysis and interpretation were performed by Sompriti Deb Roy. The first draft of the manuscript was written by Sompriti Deb Roy, and all authors commented on previous versions of the manuscript. All authors reviewed the manuscript critically and approved the final manuscript. The individual contributions of all authors are as follows. S.D.R.: Conceptualization, Methodology, Design, Visualization, Formal Analysis and investigation, Writing - original draft preparation, Reviewing and editing. V.A.: Conceptualization, Methodology, Design, Visualization, Data Curation, Writing - Reviewing and editing. B.M.: Conceptualization, Methodology, Design, Visualization, Writing - Reviewing and editing, Resources

Data and Material availability

The datasets generated or analyzed, and the materials used during the current study, are available from the corresponding author on reasonable request.

Ethics approval

Not Applicable

Consent to participate

Not Applicable

Consent to publish

Not Applicable

Acknowledgements

We want to thank Dr. G.Beig for his valuable insights during the preparation of the manuscript. We are thankful to Dr. Latha RadhaDevi for her kind help in the compilation of the MAPAN (Modeling Air Pollution and Networking) data. We wish to thank Dr. Sachin D. Ghude for his kind support, cooperation, and valuable feedback for this work. All Authors are thankful to IITM for the logistical and administrative support. We thank all the scientists who were involved in the installation and maintenance of the AQMS (Air Quality Monitoring Station) at Mahabaleswar. We would like to thank MoES (Ministry of Earth Sciences) for the financial support of the MAPAN data.

References

1. Anagha, K. S. & Kuttippurath, J. Rising ozone pollution as a threat to wheat yield in India: insights from a concentration-based approach. *Environ. Sci. Processes Impacts* (2026). http://dx.doi.org/10.1039/D5EM00850F.

2. Liu, H. et al. Ozone pollution induced-yield loss of major staple crops in China and effects from COVID-19. *J. Environ. Sci.* **157**, 804–820 (2025). https://doi.org/10.1016/j.jes.2025.02.034.

3. Ramya, A. et al. Effect of ozone stress on crop productivity: A threat to food security. *Environ. Res.* **236(2)**, 116816 (2023). https://doi.org/10.1016/j.envres.2023.116816.

4. Liu, Z. & Lu, Q. Ozone stress and crop harvesting failure: Evidence from US food production. *Food Policy* **121**, 102540 (2023). https://doi.org/10.1016/j.foodpol.2023.102540.

5. Yuan, X. et al. Concentration- and flux-based dose-responses of isoprene emission from poplar leaves and plants exposed to an ozone concentration gradient. *Plant Cell Environ.* **40**, 1960–1971 (2017).

6. Wang, T. et al. Ozone pollution in China: A review of concentrations, meteorological influences, chemical precursors, and effects. *Sci. Total Environ.* **575**, 1582–1596 (2017).

7. Malley, C. et al. Tropospheric Ozone Assessment Report: Present-day tropospheric ozone distribution and trends relevant to vegetation. *Elementa: Sci. Anthropocene* **6**, 25 (2018).

8. Van Dingenen, R. et al. TM5-FASST: A global atmospheric source-receptor model for rapid impact analysis of emission changes on air quality and short-lived 400 climate pollutants. *Atmos. Chem. Phys.* **18(21)**, 16173–16211 (2018). doi:10.5194/acp-18-16173-2018.

9. Lesser, V. M., Rawlings, J. O., Spruill, S. E. & Somerville, M. C. Ozone effects on agricultural crops: statistical methodologies and estimated dose–response relationships. *Crop Sci.* **30**, 148–155 (1990).

10. U.S. EPA. *Air Quality Criteria for Ozone and Related Photochemical Oxidants*. Report No. EPA/600/P-93/004aF (U.S. Environmental Protection Agency, 1996).

11. Mills, G. et al. A synthesis of AOT40-based response functions and critical levels for ozone for agricultural and horticultural crops. *Atmos. Environ.* **41**, 2630–2643 (2007).

12. Tong, D. Q. et al. Vegetation exposure to ozone over the continental United States: Assessment of exposure indices by the Eta-CMAQ air quality forecast model. *Atmos. Environ.* **43**, 724–733 (2009a).

13. Munir, S., Chen, H. & Ropkins, K. Non-parametric nature of ground-level ozone and its dependence on nitrogen oxides (NOx): a view point of vehicular emissions. *WIT Trans. Ecol. Environ.* **147**, 93–104 (2011).

14. Akimoto, H. et al. Analysis of monitoring data of ground-level ozone in Japan for long-term trend during 1990–2010: Causes of temporal and spatial variation. *Atmos. Environ.* **102**, 302–310 (2015).

15. Nair, P. R., Ajayakumar, R. S., David, L. M., Girach, I. A. & Mottungan, K. Decadal changes in surface ozone at the tropical station Thiruvananthapuram (8.542°N, 76.858°E), India: Effects of anthropogenic activities and meteorological variability. *Environ. Sci. Pollut. Res.* **25**, 14827–14843 (2018).

16. Ghude, S. D. et al. Reductions in Indian crop yield due to ozone. *Geophys. Res. Lett.* **41**, 51971, 5685–5691 (2014). doi: 10.1002/2014GL060930.

17. Debaje, P. K. Estimated crop yield losses due to surface ozone exposure and economic damages in India. *Environ. Sci. Pollut. Res.* **21**, 7329–7338 (2014).

18. Sinha, B. et al. Assessment of crop yield losses in Punjab and Haryana using 2 years of continuous in situ ozone measurements. *Atmos. Chem. Phys.* **15**, 9555–9576 (2015).

19. Sharma, A., Ojha, N., Pozzer, A., Beig, G & Gunthe, S. S. Revisiting the crop yield loss in India attributable to ozone. *Atmos. Environ. **X*** **1**, 100008 (2019). https://doi.org/10.1016/j.aeaoa.2019.100008.

20. Deb Roy, S., Beig, G., Bano, S. & Murthy, B. Impact assessment of surface ozone exposure on crop yields at three tropical stations over India. *Environ. Monit. Assess.* **195**, 338 (2023). https://doi.org/10.1007/s10661-022-10889-w.

21. Dewan, S. & Lakhani, A. Impact of ozone pollution on crop yield, human health, and associated economic costs in the Indo-Gangetic plains. *Sci. Total Environ.* **945**, 173820 (2024). https://doi.org/10.1016/j.scitotenv.2024.173820.

22. Jain, S. L., Arya, B. C., Kumar, A., Ghude, S. D. & Kulkarni, P. S. Observational study of surface ozone at New Delhi, India. *Int. J. Remote Sens.* **26(16)**, 3515–3524 (2005). doi:10.1080/01431160500076616.

23. Kutal, G. et al. Characteristics of Surface Ozone Levels at Climatologically and Topographically Distinct Metropolitan Cities in India. *Asian J. Atmos. Environ.* **16(2)**, 2022004 (2022). doi: https://doi.org/10.5572/ajae.2022.004.

24. Chand, D. & Lal, S. High ozone at rural sites in India. *Atmos. Chem. Phys. Discuss.* **4**, 3359–3380 (2004). Doi: 10.5194/acpd-4-3359-2004.

25. Naja, M., Chand, D., Sahu, L. & Lal, S. Trace gases over marine regions around India. *Indian J. Geo-Mar. Sci.* **33**, 99–106 (2004).

26. Kumar, R., Naja, M., Pfister, G. G., Barth, M. C. & Brasseur, G. P. Source attribution of carbon monoxide in India and surrounding region during wintertime. *J. Geophys. Res. Atmos.* **118**, 1981–1995 (2013). doi:10.1002/jgrd.50134.

27. Naja, M., Lal, S. & Chand, D. Diurnal and seasonal variabilities in surface ozone at a high altitude site Mt Abu (24.6°N, 72.7°E, 1680m asl) in India. *Atmos. Environ.* **37**, 4205–4215 (2003). doi:10.1016/S1352-2310(03)00565-X.

28. Kumar, R., Naja, M., Venkataramani, S. & Wild, O. Variations in surface ozone at Nainital: A high-altitude site in the central Himalayas. *J. Geophys. Res.* **115**, D16302 (2010). doi:10.1029/2009JD013715.

29. Buchunde, P. et al. Characterisation of particulate matter at a high-altitude site in southwest India: Impact of dust episodes. *J. Earth Syst. Sci.* **128**, 237 (2019). https://doi.org/10.1007/s12040-019-1265-8.

30. Leena, P. P., Vijayakumar, K., Anilkumar, V. & Pandithurai, G. Analysing temporal variability of particulate matter and possible contributing factors over Mahabaleshwar, a high-altitude station in Western Ghats, India. *J. Atmos. Sol.-Terr. Phys.* **164**, 105–115 (2017).

31. Kutal, G., Kolhe, A., Varpe, S. & Aher, G. An investigation of temporal variability of the total column ozone over tropical urban, high altitude, and coastal stations in Western Maharashtra, India. *Int. J. Remote Sens.* **38**, 1197–1223 (2017).

32. Environnement S.A. *UV Photometric Ozone Analyser, Technical Manual (O342 Module)* (Environnement S.A., 2002). http://www.environnement-sa.com.

33. Mallik, C., Lal, S. & Venkataramani, S. Trace gases at a semi-arid urban site in western India: variability and inter-correlations. *J. Atmos. Chem.* **72**, 143–164 (2015).

34. Rana, M., Mittal, S. K. & Beig, G. Enhanced Ozone Production in Ambient Air at Patiala Semi-Urban Site During Crop Residue Burning Events. *MAPAN-J. Metrol. Soc. India* **34(2)**, 273–288 (2019). Doi: 10.1007/s12647-019-00315-x.

35. Rahman, W., Beig, G., Barman, N., Hopke, P. K. & Hoque, R. R. Ambient ozone over mid-Brahmaputra Valley, India: effects of local emissions and atmospheric transport on the photostationary state. *Environ. Monit. Assess.* **193**, 790 (2021). doi:10.1007/s10661-021-09572-3.

36. Latha, R. et al. On the transition of major pollutant and O3 production regime during Covid-19 lockdowns. *J. Environ. Manag.* **328** (2023), 116907, https://doi.org/10.1016/j.jenvman.2022.116907.

37. Deb Roy, S., Beig, G. & Ghude, S. D. Exposure-plant response of ambient ozone over the tropical Indian region. *Atmos. Chem. Phys.* **9**, 5253–5260 (2009). doi: 10.5194/acp-9-5253-2009.

38. Lal, S. et al. Loss of crop yields in India due to surface ozone: an estimation based on a network of observations. *Environ. Sci. Pollut. Res.* **24(26)**, 20972–20981 (2017). https://doi.org/10.1007/s11356-017-9729-3.

39. Tsutsumi, Y., Zaizen, Y. & Makino, Y. Tropospheric ozone measurement at the top of Mt. Fuji. *Geophys. Res. Lett.* **21**, 1727–1730 (1994). doi:10.1029/94GL01107.

40. Mao, J., Feng, Z. & Tai, A. P. K. Impacts of surface ozone pollution on wheat production in China from 2005 to 2019: A comparison among different methodologies for ozone-crop relationships. *Atmos. Environ.* **360**, 121413 (2025). https://doi.org/10.1016/j.atmosenv.2025.121413.

41. Peng, J., Shang, B., Xu, Y., Feng, Z. & Calatayud, V. Effects of ozone on maize (*Zea mays* L.) photosynthetic physiology, biomass and yield components based on exposure- and flux-response relationships. *Environ. Pollut.* **256**, 113466 (2020). https://doi.org/10.1016/j.envpol.2019.113466.

42. Hollaway, M. J., Arnold, S. R., Challinor, A. J. & Emberson, L. D. Intercontinental trans-boundary contributions to ozone-induced crop yield losses in the Northern Hemisphere. *Biogeosciences* **9**, 271–292 (2012). doi:10.5194/bg-9-271-2012.

43. Van Dingenen, R. et al. The global impact of ozone on agricultural crop yields under current and future air quality legislation. *Atmos. Environ.* **43**, 604–618 (2009).

44. Avnery, S., Mauzerall, D.L., Liu, J. & Horowitz, L.W. Global crop yield reductions due to surface ozone exposure: 1. Year 2000 crop production losses and economic damage. *Atmos. Environ.* **45**, 2284–2296(2011a). doi:10.1016/j.atmosenv.2011.01.045.

45. Avnery, S., Mauzerall, D.L., Liu, J. & Horowitz, L.W. Global crop yield reductions due to surface ozone exposure: 2. Year 2030 potential crop production losses and economic damage under two scenarios of O_3 pollution. *Atmos. Environ.* **45**, 2297–2309(2011b). doi:10.1016/j.atmosenv.2011.01.00.

46. Oltmans, S. J. & Levy II, H. Surface ozone measurements from a global network. *Atmos. Environ.* **28**, 9–24 (1994). doi:10.1016/1352-2310(94)90019-1.

47. Galanter, M., Levy II, H. & Carmichael, G. R. Impacts of biomass burning on tropospheric CO, NOx, and O3. *J. Geophys. Res.* **105**, 6633–6653 (2000). https://doi.org/10.1029/1999JD901113.

48. Emberson, L. D. et al. A comparison of North-American and Asian exposure-response data for ozone effects on crop yields. *Atmos. Environ.* **43**, 1945–1953 (2009).

49. Oksanen, E. et al. Impacts of increasing ozone on Indian plants. *Environ. Pollut.* **177**, 189–200 (2013).

50. Pei, J. et al. Interactive effects of ozone pollution and atmospheric drought on crop yields: A spatially explicit assessment. *J. Environ. Sci.* (2026). https://doi.org/10.1016/j.jes.2026.01.059.